J. Min. Metall. Sect. B-Metall. 48 (1) B (2012) 101 - 113

Journal of
Mining and
Metallurgy

X-RAY DIFFRACTION AND SEM/EDX STUDIES ON TECHNOLOGICAL EVOLUTION OF THE OXIDE-FLUORIDE CERAMIC FLUX FOR SUBMERGED ARC-SURFACING

V.E. Sokolsky[*,#], A.S. Roik[*], A.V. Davidenko[*], V.P. Kazimirov[*], V.V. Lisnyak[*,#], V.I. Galinich[**], I.A. Goncharov[**]

[*]Physical Chemistry Chair, Chemical Department, Kyiv National Taras Shevchenko University, Kyiv, Ukraine
[**]The E.O. Paton Electric Welding Institute, Kyiv, Ukraine

(Received 23 December 2010; accepted 14 July 2011)

Abstract

The ceramic flux for submerged arc-surfacing with main component composition MgO (10.0 wt. %)–Al_2O_3 (25.0 wt. %)–SiO_2 (40.0 wt. %)–CaF_2 (25.0 wt. %) was prepared in a disk dryer-granulator using a sodium/potassium silicate solution as a binder. X-ray powder diffraction (XRPD) collected at r.t. identified α-phase of quartz, Al_2O_3, MgO and CaF_2 of the initial components in the samples taken after granulation and subsequent annealing at 600 °C. In contrast to the low temperature annealing, anorthite ($CaAl_2Si_2O_8$) is the main phase in the composition of the samples remelted at 1500 °C and quenched subsequently. Chemical analysis performed by means of scanning electron microscopy with energy-dispersive X-ray spectroscopy analysis (SEM/EDX) detects that the grains of the remelted samples possess the same Ca : Al : Si elemental ratio as anorthite. High temperature X-ray diffraction (HTXRD) was used to examine structural transformation in the solid at 600 °C < T < 1200 °C and stages of thermal evolution of ceramic flux were determined. The ceramic flux melts completely at the temperature above 1350 °C. The intensity pattern of the flux melt was obtained by X-ray diffraction of scattered X-rays at 1450 °C. After calculating the structure factor (SF), the radial distribution function (RDF) was evaluated and used to calculate the structural basicity of the flux melt.

Keywords: Ceramic flux; Submerged arc-surfacing; Structure; Scanning electron microscopy, Energy-dispersive X-ray spectroscopy; High-temperature X-ray diffraction; Anorthite

[#] *Corresponding author: sokol@univ.kiev.ua (V.E.Sokolsky) and lisnyak@Chem.univ.kiev.ua (V.V. Lisnyak)*

DOI:10.2298/JMMB101223002S

1. Introduction

The submerged-arc surfacing (SAS) due to its operational facilities is widely used efficient technique of depositing a layer of material onto the surface of a steel to make it more resistant to wear, corrosion or high temperature treatment [1–4]. Also strengthening of material surface can be achieved by electric arc overlaying; this process enables to obtain thick layers of various composition and properties on the surface of the structural parts. This enhances production economies by enabling the use of a cheaper, more easily workable parent material coated with expensive metals and alloys to achieve desired characteristics. The granulated ceramic flux partially or completely melts and generates a liquid protective slag layer, which is solidified subsequently [5–7]. The fluxes that originate the slag can be classified by chemical activity of the interaction with the surfaced metal using the basicity parameter [8, 9].

Among known fluxes for SAS the oxide-fluoride ceramic fused fluxes are widely used in Ukraine for the surfacing of metal at metalwork production. However, processes, which occur at heating and melting of flux, are practically beyond of comprehensive examination.

The main objective of this work is to study the technological evolution of the oxide-fluoride ceramic flux using scanning electron microscopy with energy-dispersive X-ray spectroscopy analysis (SEM/EDX) and X-ray diffraction. Emphasis is given to the ceramic flux transformation at heating. The examination of thermal evolution of oxides, which are included in the ceramic fluxes, is closely related to the most recent studies devoted to the thermal degradation [10] and to the effect of the fluxing components on the liquidus and phase relations of the fluxes [11].

2. Experimental

2.1. Preparation

The preset quantities of powdered main components (10% mass. MgO, 25% mass. Al_2O_3, 40% mass. SiO_2 and 25% mass. CaF_2) were mixed mechanically. A sodium/potassium silicate solution (so-called liquid glass), with a dry content of 40-60%, used as a binder, was continuously supplied to the disk dryer-granulator. The grains were sifted through sieves and annealed at 600 °C. The prepared granulated and annealed powder ceramic flux was remelted at 1500 ^oC in Mo crucible and the samples taken from the upper and the inner parts of the crucible were subjected to the further examinations.

2.2. Characterization

The room temperature X-ray powder diffraction (XRPD) data of the granulated and dried samples of the flux as well as the remelted samples taken from the upper and the inner parts of the Mo crucible were collected by means of a DRON-3M powder diffractometer using Ni-filtered CuKα-radiation (λ = 1.5418 Å, U = 30 kV, I = 30mA). The data were scanned over the angular range 10–100°(2θ) with a step size of 0.02°(2θ) and a counting time of 1 sec. PowderCell 2.4 software package [12, 13]

was used for the data evaluation. The phase identification and quantitative X-ray diffraction phase analysis (QXRPD) were performed by using Match software [14].

The high temperature X-ray diffraction (HTXRD) studies were performed to examine the thermal evolution of the oxide-fluoride ceramic flux. X-ray patterns have been obtained using a high-temperature θ–θ diffractometer operated with MoKα radiation (λ = 0.7107 Å). The Zr–Y differential filters were used for monochromatization of X-ray radiation, which was reflected from the horizontal surface of solid powdered oxide-fluoride ceramic flux or from the free surface of the liquid oxide-fluoride ceramic flux. The sample in the molybdenum crucible was situated on the desktop of the high-vacuum chamber of the diffractometer. Before the sample was heated to the experimental temperature by a special resistant heater the chamber inner volume was vacuumized and filled with pure helium. Measurements and control of temperature was performed using thermopiles with an uncertainty of measurement of less than ±3 K at the 95% confidence level. The intensity patterns were recorded at temperatures of 600, 800, 1000, 1200, 1350 and 1450 °C. The apparatus, measurement and calculation routines were reported in [15].

Powdered sample of flux fixed on the graphite substrate were examined with a Jeol scanning electron microscope JSM 7700 F (SEM) operating at 5 kV. An Oxford spectrometer, attached to the 7700 F, was used for energy dispersive X-ray (EDX) microanalysis. To prevent charges caused by the electron beam in the low conductive solid flux samples, 3 nm thick layer of pure platinum was sputtered on the surface of the samples. The total chemical composition of ceramic flux mixture after annealing at 600 °C was determined by X-rays fluorescence spectrometry (XRF) with a Philips X'Unique II (model 1480) wavelength-dispersive XRF spectrometer. The spectrometer was equipped with a rhodium X-ray tube, operated at 50 kV and 40 mA.

3. Results and Discussion

3.1. Characterization of granulated and annealed powder ceramic flux

The theoretical content of components in the mixture for preparation of the ceramic flux and the experimental content of components in the obtained annealed mixture, by the XRF data, were listed in Table 1.

The initial components alpha quartz, trigonal phase of Al_2O_3, cubic MgO and

Table 1. Composition of ceramic flux.

	Composition, mass. %						
	MgO	Al_2O_3	SiO_2	CaF_2	Na_2O	K_2O	Fe_2O_3*
Calc.	10	25	40	25			
Found	8.9	22.6	42	21.9	1.4	0.8	1.4

*Note: * corresponds to the content of Fe_2O_3 admixture*

CaF_2 phases were determined by XRPD in the samples after granulation and annealing at 600 °C (Fig. 1) and no other crystalline products including that based on the liquid glass were found [16, 17].

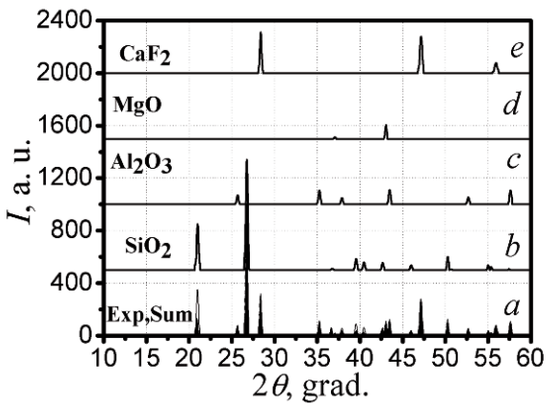

Fig. 1. Experimental powder diffraction pattern of powdered ceramic flux and summarized curve fitted with Powdercell (a). The fit is based on the reflections of α-quartz (SiO_2) (b), corundum Al_2O_3 (c), periclaz MgO (d) and fluorite CaF_2 (e) phases.

According to the results of the EDX/SEM microanalysis, performed on the powdered samples, it was found that composition of the main phases is equal to that of the initial components (MgO, Al_2O_3, SiO_2 and CaF_2). No phases, which composition show pronounced difference from stated, were registered for the ceramic flux after granulation and subsequent samples annealing at 600 °C.

3.2. Characterization of remelted powder ceramic flux

The SEM microphotos and EDX microanalysis data were represented in Table 2. The SEM microphotos of the samples were taken from the upper and from the inner part of the molybdenum crucible differ significantly. Blisters, where gas bubbles accumulate, micro-cracks *etc*. are clearly seen on the SEM microphotos. These features testify on a good separation of the slag coverage from the inner part of the crucible. The samples are inhomogeneous with respect to fluorine content, the latter concentrate at the inner part of the crucible. The fluorine content can be more than 7 at. %, if one omit the amount of fluorine in the blisters (Table 2, microphoto 1–2), the upper part contains less fluorine *c.a*. 0.99–3.50 at. % (Table 2, microphoto 3–4). It can be seen also bright blotches (Table 2, microphoto 1, spectra 3–4; microphoto 2, spectrum 3) containing a considerable amount of fluoride, but the surface area of these particles is negligible.

It should be pointed the fact (Table 2, microphoto 1, spectrum 2; microphoto 2, spectra 1, 2, 4 and microphoto 3–4 all spectra) that the approximate ratio of components in the majority of analysis is Ca : Al : Si = 1 : 2 : 2, the latter corresponds to $Ca(Al_2Si_2O_8)$ anorthite. The content of sodium determined by SEM/EDX in these samples is much lower than in the samples before melting. This means that the sodium is uniformly distributed over the volume after melting and subsequent quenching of remelted flux. The fluorine content (C_F) is in the range 3–16 at. % at the samples, which are taken from the inner part of the crucible. Whereas, C_F is found to be below 3.5 at. % at the samples taken from the upper part of the crucible. It was found that the inner part of the crucible contains significantly more

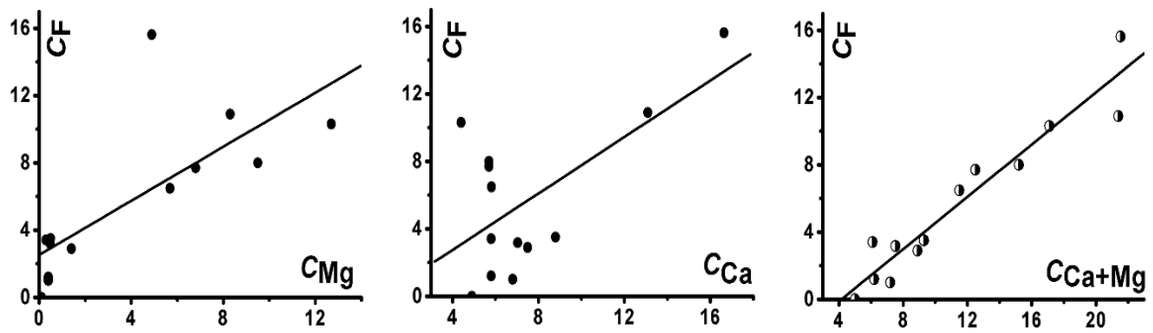

Fig. 2. The dependence of the fluorine content (C_F) on a) C_{Mg}; b) C_{Ca} and c) $C_{Ca + Mg}$.a

Mg than the upper part. Fig. 2 shows the dependence of fluorine content (C_F) on magnum (C_{Mg}), calcium (C_{Ca}) and their sum (C_{Ca} + C_{Mg}), for all data obtained by the SEM/EDX (both from the inner and upper parts). The linear correlation at the $C_F - (C_{Ca} + C_{Mg})$ dependence can indicate that the fluorine is partially redistributed between Ca and Mg, which in turn implies transformation of CaF_2 into CaO and the anorthite as well as transformation of MgO into MgF_2.

The QXRPD of the ceramic flux remelted at 1500 °C sample (Fig. 3) shows that the main phases in the samples from both crucible sides are triclinic (a = 0.8192 nm, b = 1.2869 nm, c = 1.4180 nm, α = 93.180°, β = 115.63°, γ = 91.080°, sp. gr. P $\bar{1}$) anorthite (PDF card No. 411486) [16] and tetragonal MgF_2 (a = 0.4615 nm, b = 0.4615 nm, c = 0.3043 nm, sp. gr. P $4_2/mnm$) (PDF card No. 722231) [16] in the ratio 95/5 % wt. The QXRPD analysis can testify that suggested transformation of MgO and CaF_2 occurs at the ceramic flux melting.

The one of the ways of the anorthite formation is thermal destruction of complex oxy-fluoride compounds (e.g., $AlCa_2Mg_5NaSi_7O_{22}F_2$) by the following reactions:

$$2AlCa_2Mg_5NaSi_7O_{22}F_2 \rightarrow CaAl_2Si_2O_8 + {+}MgF_2 + 3CaMg_3Si_4O_{12} + 2NaF \quad ...(1)$$

$$2AlCa_2Mg_5NaSi_7O_{22}F_2 \rightarrow CaAl_2Si_2O_8 + 2MgF_2 + Ca_3Mg_8Si_{12}O_{35} + Na_2O \quad \ldots(2)$$

$$2AlCa_2Mg_5NaSi_7O_{22}F_2 \rightarrow CaAl_2Si_2O_8 + MgF_2 + 3CaO + 9MgO + 12SiO_2 + 2NaF \quad \ldots(3)$$

$$2AlCa_2Mg_5NaSi_7O_{22}F_2 \rightarrow CaAl_2Si_2O_8 + 2MgF_2 + 3CaO + 8MgO + 12SiO_2 + Na_2O \quad \ldots(4)$$

The fluorine and oxygen atoms in the crystalline structures of the major of complex oxy-fluoride compounds [17] are nearest-neighbors of Mg^{2+} and Ca^{2+}, respectively, so, MgF_2 and CaO can be formed at the thermal decomposition of these compounds and further the phase separation can be implied.

These oxy-fluoride compounds can be formed by the products of liquid glass decomposition and by the compounds formed at the boundary layers of several components of the flux. The compounds can exist in amorphous and quasi-amorphous

Table 2. Microphotos and data of EDX microanalysis of the remelted ceramic surfacing flux.

The sample taken from the inner part of the crucible, microphoto 1.					
Spectrum	1	2	3	4	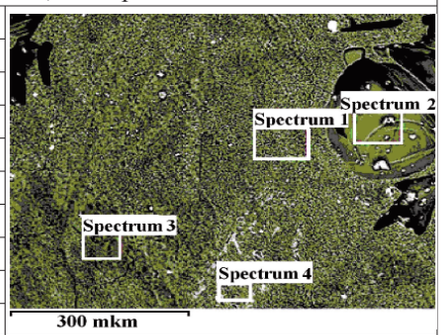
Element, at., %					
O	58.9	67.6	56.3	54	
F	8	3.4	10.3	10.9	
Na	0.2	0.3	0.4	0	
Mg	9.5	0.3	12.7	8.3	
Al	6.7	12	5.8	2.3	
Si	11	11.1	10.1	11.4	
Ca	5.7	5.8	4.4	13.1	
Ti			< 0.1		
Composition		$CaAl_2Si_2O_8$			
The sample taken from the inner part of the crucible, microphoto 2.					
Spectrum	1	2	3	4	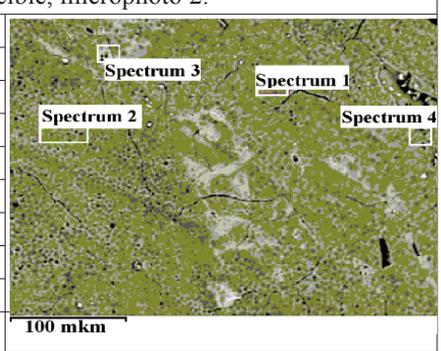
Element, at., %					
O	59.7	60.92	51.55	63.29	
F	7.7	6.48	15.63	3.17	
Na	0.1	0.14	0	0.02	
Mg	6.8	5.69	4.89	0.49	
Al	8.8	9.48	1.22	13.25	
Si	11.1	11.47	10.08	12.74	
Ca	5.7	5.81	16.64	7.04	
Composition	$CaAl_2Si_2O_8$	$CaAl_2Si_2O_8$		$CaAl_2Si_2O_8$	
The sample taken from the upper part of the crucible, microphoto 3.					
Spectrum	1	2	3		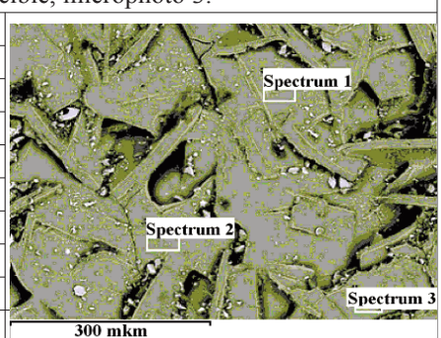
Element, at., %					
O	62.6	66	60.9		
F	2.9	1	3.5		
Na	0.1	0.3	0.3		
Mg	1.4	0.4	0. 5		
Al	12.8	12.8	13.5		
Si	12.7	12.6	12.6		
Ca	7.5	6.8	8.8		
Composition	$CaAl_2Si_2O_8$	$CaAl_2Si_2O_8$	$CaAl_2Si_2O_8$		
The sample taken from the upper part of the crucible, microphoto 4.					
Spectrum	1	2			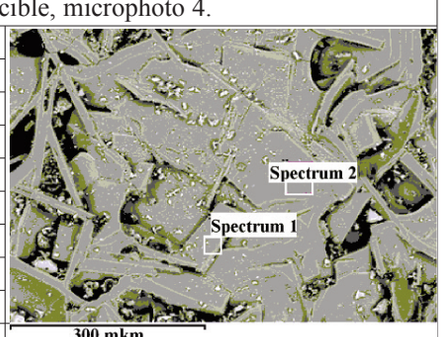
Element, at., %					
O	72.1	67.9			
F	-	1.2			
Na	0.1	0.1			
Mg	0.1	0.4			
Al	11.7	12.5			
Si	11.1	12.1			
Ca	4.9	5.8			
Composition	$CaAl_2Si_2O_8$	$CaAl_2Si_2O_8$			

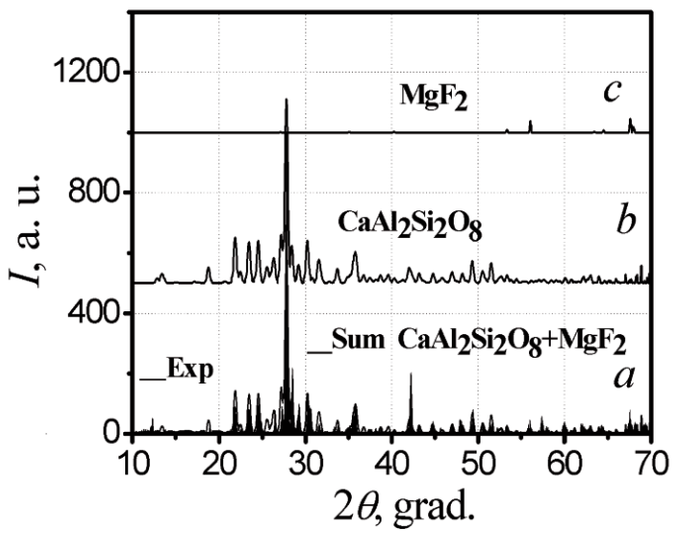

Fig. 3. Powder diffraction pattern of the flux remelted at 1500 °C from the inner part of the crucible a) the experimental and the sum pattern of triclinic $CaAl_2Si_2O_8$ and MgF_2 (line with shaded area under the curve) refined profile of anorthite b) and magnesium fluoride c).

state in the ceramic flux as no additional reflections of the other phases were observed in the XRPD patterns. So, one can expect the formation of MgF_2, CaO and anorthite by transformations of oxide-fluoride moieties at the thermal decomposition of the complex compounds at the least on the theory level.

It is not ruled out that the formation of magnesium fluoride and anorthite occurs by other mechanisms. Anorthite is sufficiently stabile and, like feldspar, belongs to one of the most common minerals of the Earth's crust. Therefore, the anorthite nuclei formed by one of the reactions (1–4) can be grown at the expense of the other components of the flux *i.e*. Al_2O_3 and SiO_2, as well as CaO, which was formed by the reactions (3–4).

To interpret the results obtained the phase diagram of the ternary CaO–MgO–Al_2O_3–SiO_2 system known form the literature [18–22] can be used instead of unexplored complex phase diagram of the Na_2O–Al_2O_3–MgO–CaO –SiO_2–CaF_2–MgF_2 system.

According to the diagram [16, 19], the crystallization field of anorthite intersects a vertical section of the phase diagram at 15 mass. % of Al_2O_3 and displaces the crystallization fields of wollastonite ($CaSiO_3$) and pyroxene ($MgSiO_3$). Only, strongly narrowed crystallization field of pyroxene intersects the section at 20 mass. % of Al_2O_3. The crystallization fields of periclase (MgO), spinel (Al_2MgO_4), cordierite ($Mg_2Al_4Si_5O_{18}$), but no that of MgO and calcium aluminate are presented at the section at 10 mass. % of Al_2O_3. According to the phase diagram of the quaternary CaO–MgO–Al_2O_3–SiO_2 system, the anorthite is formed at the low content of MgO (10–15% at.), while the spinel is formed at the high content of periclase.

3.3. The high temperature X-ray diffraction (HTXRD) studies

According to results of the HTXRD patterns analysis, the phase transformations of the initial components (e.g. α-phase of quartz) are occurred in the solid state at the temperature below 1200 °C (Fig. 4). Complex compounds ($AlCa_2Mg_5NaSi_7O_{22}F_2$), which are based on the decomposition products of liquid glass and its surrounding of the flux component, are probably formed at the lower temperature. The sample partially melts at 1200 °C, and contains a certain amount of the crystalline phase. The MgF_2 phase is extremely thermostable and exists in the sample at the whole temperature interval. This phase coexists with the anorthite at 1200 °C and with the liquid phase and 1350 °C. Fig. 4b shows results of the simulation of the HTXRD pattern of the sample, which contains MgF_2 and anorthite. As one can see from the Fig. 3b, these phases identification is complicated by the fact that their reflections overlap due to effect of the temperature factor.

Summarizing data discussed previously, one can assumed that heating above 500 °C is greatly intensified the diffusion on the phase interface. So, the surface layers enriched with the interface reacting phases, the latter are based on the products of the liquid glass thermal destruction, are formed on the granules of the main components. Further heating up to 1450 °C leads to formation of the more complex chemical compounds by the interaction of boundary layers of the main components within the binding matrix. Subsequent temperature

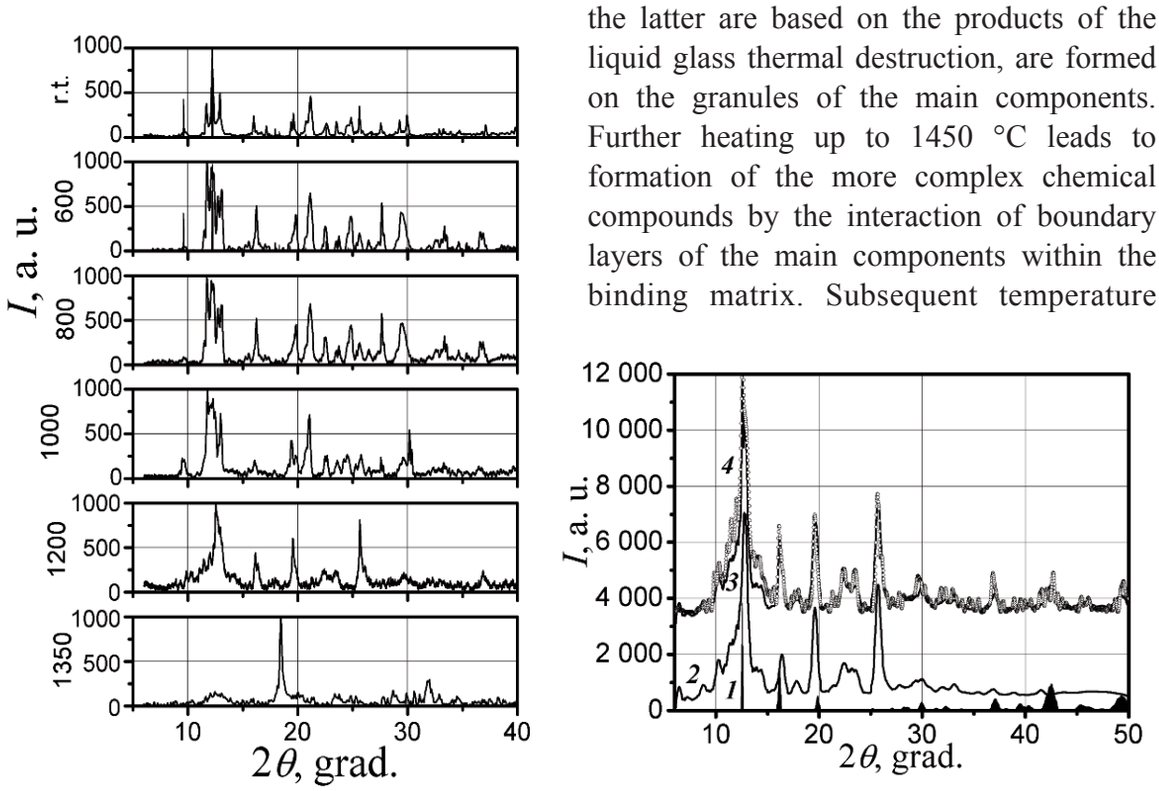

Fig. 4. a) The X-ray diffraction patterns of the flux measured at the different temperature b) The X-ray diffraction patterns of MgF_2 (1) and of $Ca(Al_2Si_2O_8)$ (2) with broadened half-width of the diffraction peaks after the profile refinement with PowderCell, the refined pattern of 1+2 sum (3), and the experimental pattern at 1200 °C (4).

increase leads to dissolution of the components at the partial melting and to the formation of local molten inclusions. The diffusion rate of the substance between the inclusions constituents increases significantly, while the diffusion between solid and liquid components shows lesser increase. Thus, a liquid matrix with partially dissolved components are composed the flux at the final stage of the technological evolution. The melting of the ceramic flux is accompanied with increase of the interaction of the liquid matrix with the components, sintering of the particles and possible partial crystallization of the matrix.

Our considerations regarding suggested stages of the technological evolution of the mixture of solid reagents in the matrix of binder can be represented as follows:

1) Granulation of the mixture of initial components in the liquid glass matrix;

2) Formation of interface compounds by the particles of components and liquid glass at the beginning of the annealing;

3) Formation of the more complex compounds of several components and the liquid glass at the ceramic flux subsequent heating up to 1450 °C;

4) Melting of the matrix based on the products of liquid glass destruction at the temperature above 1450 °C.

3.3. Characterization of molten ceramic flux

The liquid phase is formed at 1450 °C. Fig. 5 shows the IC of the molten sample recorded at 1450 °C, SF calculated from IC, and RDF curves. As can be seen from Fig. 5b, the first SF maximum is located at ~2 nm^{-1}, which is uncommon and observed preferentially for complex oxide melts.

To classify the ceramic flux on a scale of acidity we determined the structural basicity instead of the optical basicity. If compared with the optical basicity, which is a chemical parameter used for slags and correlates with such important physical property of slags as viscosity [23, 24], the structural basicity is more precise as obtained directly from X-ray structural data [25].

The main idea of structural basicity determination is based on a fact that one can find the most probable nearest inter-atomic distances and the values of the area under maxima from experimental RDF. These structure-related RDF features are additively interrelate with coordination numbers of the atoms being components of oxide melts [26], so empirical relation can be proposed. The most of the known expressions for the determination of basicity in general form can be written as

$$B = \frac{\sum_{i=1}^{L_1} p_i \mathrm{Me}_x\mathrm{O}_y + \sum_{i=1}^{L_2} p_i \mathrm{Me}_x\mathrm{F}_y}{\sum_{i=1}^{K} p_i \mathrm{Me}_x\mathrm{O}_y} \qquad \ldots(5)$$

where $\mathrm{Me}_x\mathrm{O}_y$ and $\mathrm{Me}_x\mathrm{F}_y$ are oxides and fluorides component, correspondingly, taking in weight or molar percents; L_1, L_2, K are quantity of basic oxides, fluorides and acidic oxides, correspondingly; p_i is the weight coefficient of the component. The weight coefficient is related to the chemical activity of each of the component. The expression in the denominator contributes to the first (acidic) RDF peak, and in the numerator to the second (basic) RDF peak.

The area under RDF associated with the

atomic fractions and the coordination number of any of the components. Contribution of coordination of metal cation–oxygen anion atomic pairs can be defined as:

$$A = 2n_C K_C K_O Z_{C(O)} \quad \ldots(6)$$

Here and below n_C, n_O are the atomic fraction of the metal cation and oxygen anion; K_C, K_O are the relative atomic factors of the metal and oxygen, respectively, averaged over the scattering angles; $Z_{C(O)}$ is the number of oxygen atoms around the metal atom cation and $Z_{O(C)}$ is the number of metal atoms around the oxygen atom. The value of area under the first peak, in which contributes only K of acidic components with taking into account their atomic fraction, can be written as:

$$A_1 = \sum_{i=1}^{k} 2n_C K_C K_O Z_{C(O)} \quad \ldots(7)$$

Analogously, the value of area under the second peak for l component of the melt can be represented as follows

$$A_2 = \sum_{i=1}^{l} 2n_C K_C K_O Z_{C(O)} \quad \ldots(8)$$

At the first glance, there is a direct relationship between the basicity and the concentrations of oxides. For some components, this observation is true, if they are typically acidic as SiO_2 or basic as Na_2O or CaO. However there is a whole group of amphoteric components, which can be either acidic or basic. These are oxides of Al, Ti, Mn and Fe. Cations of these oxides serve a dual function depending on their location in an oxygen matrix [27, 28]. The concept of acid and basic components is conventional, since silicon oxide in the general case amphoteric, but it can be basic in the presence of more acidic oxides.

Comparative analysis using Shannon and Prewitt ionic radii leads to the following results [26, 29]. The cation-oxygen pairs, where the cations have a small ionic radius (0.04–0.08 nm), high (3+, 4+) oxidation degree, large force field and the coordination number (CN) of the cation to oxygen close to 4, contributes to the first RDF maximum. The second RDF maximum is realized due to contribution of the cation-anion pairs, where the cations have large ionic radii (0.08–0.12 nm), low oxidation degree (1+, 2+), low force field strength, and their coordination with oxygen can be estimated as octahedral (CN = 6). The first maximum of the RDF curve of examined slag melts forms mainly due to the contributions of silica and alumina, but in the most cases, the area under the first peak slightly higher than that found from the contribution of these two oxides. The area under the second RDF maximum formed due to the contribution of oxides of lithium, sodium, potassium, magnesium, calcium, iron and manganese, is slightly less then that calculated by Eqn. (8). This means that part of these oxides, which contribute into the second peak, can contribute to the first peak. So, the changes of the area under the first and under the second peak are interconnected.

In the case of significant Al_2O_3 content in the slag melts, the increase of the area under the first peak leads to a subsequent increase of the area under the second peak.

Thus in all other cases, the growth of the area under the first peak is accompanied by a

decrease of the area under the second peak. The contribution of any coordination in the RDF profile at the range of these two peaks can be described by a Gaussian-type curve

$$\phi_i(R) = \frac{A_i}{\sigma_i\sqrt{2\pi}} \cdot \exp\left(-\frac{(R-R_o)^2}{2\sigma_i^2}\right) \quad \ldots(9)$$

Consequently, the complete RDF profile can be described by a sum of mentioned Gaussian curves as follows:

$$\phi_i(R) = \sum_{i=1}^{R} \frac{A_i}{\sigma_i\sqrt{2\pi}} \cdot \exp\left(-\frac{(R-R_{io})^2}{2\sigma_i^2}\right) \quad \ldots(10)$$

where R_{io}, σ_i are the location and the dispersion of peak of *i*-coordination, respectively.

Further, the RDF profile for the range of the first and the second peaks was optimally fitted by changing in possible limits the peaks positions, heights and dispersions. The value of σ_i for each of coordination was determined from the condition of the best coincidence of theoretical (expected) and experimental RDF in the range which is corresponded to the first two maxima.

The structural basicity was calculated by using the X-ray diffraction data of X-rays scattered form the free surface of the molten ceramic flux [15]. From the chemical composition of the flux one can suggested that oxides MgO, Na_2O, CaO (probably formed by the oxyfloride complex compounds) and in a part Al_2O_3, which can contribute simultaneously as acid and base, mainly contribute into the flux basicity. The total contribution of the coordination of each oxide used in this calculation perfectly fits the RDF profile at the region of the first two structural peaks (Fig. 5d). According to the calculations, the main contribution into the basicity is paid by 0.77 % of CaO, by 0.52 % of Al_2O_3 and by 0.7 % MgO.

The acidic fraction in the basicity calculation consists of mainly contributions of 100% SiO_2 and 48% Al_2O_3. According to our data only 20 % of calcium ions form calcium fluoride. If one considers fluorides (CaF_2 and MgF_2) as neutral components, the basicity of the flux can be calculated as follows

$$B = (0.77C_{CaO} + C_{Na_2O} + C_{K_2O} + 0.52C_{Al_2O_3} + 0.2C_{MgO} + 0.5C_{Fe_2O_3}) / (C_{SiO_2} + 0.48C_{Al_2O_3} + 0.5C_{Fe_2O_3}) = 0.47 \quad \ldots(11)$$

where C_{MgO}, C_{CaO}, C_{MgO}, C_{oxide}, *etc*. are the mass. % of the basic and acidic component, which are in the numerator and the denominator of the formula, respectively.

It should be noticed that the calculation of the basicity was performed using only the data of X-ray diffraction for X-rays scattered from the surface of the melt. However, the chemical composition of the inner and upper parts of the melt in the crucible differs significantly, as it was shown by subsequent SEM/EDX studies. The lowering of oxide and increasing of fluoride content from upper to inner parts of the flux in the crucible (Table 2) means that the inner parts can show higher oxide and lower fluoride contribution into the basicity. So, one can assume that the molten flux should be more acidic at the zone of contact with the metal at the SAS.

4. Conclusions

This study demonstrates the complex nature of the interaction in surfacing ceramic flux before the formation of the molten flux. The major structural changes at the flux heated below 1200 °C occur due to the solid-

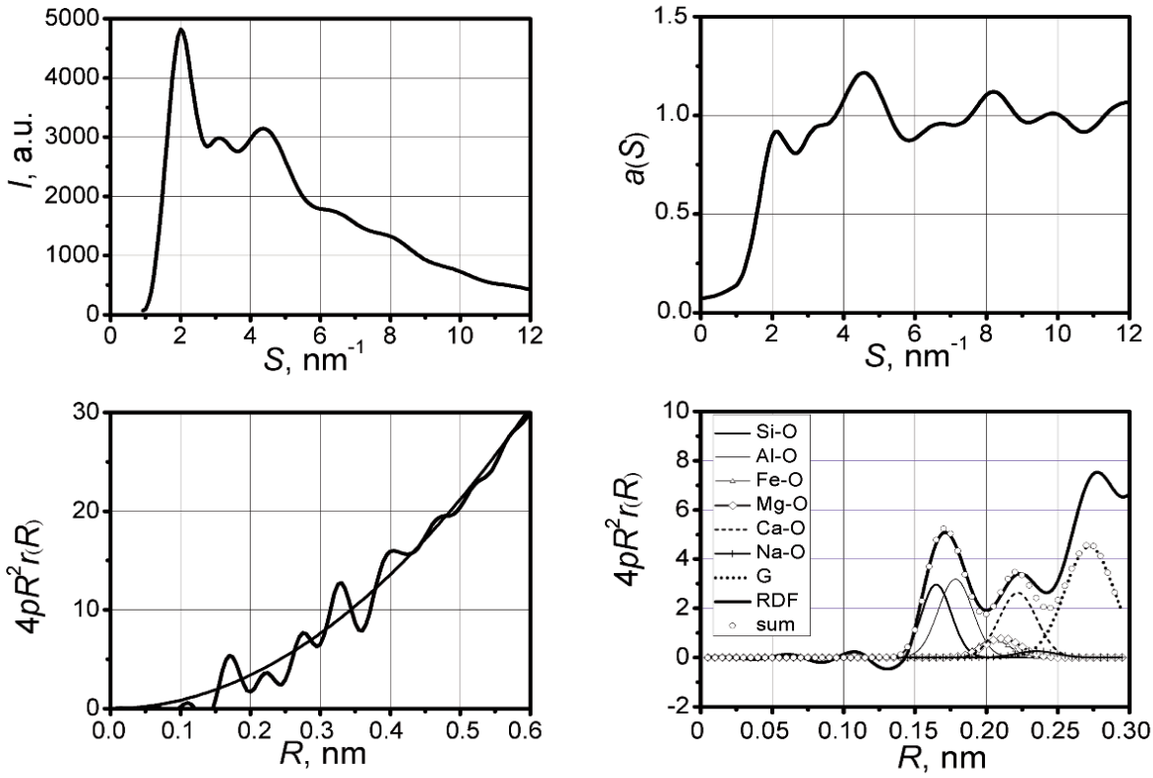

Fig. 5. The structural characteristics of the molten flux: a) the intensity curve (IC) of the scattered X-rays; b) the structure factor (SF); c) the curve of the radial distribution function (RDF); deconvolution of RDF at the first and the second diffraction peak by area.

state interactions of the sintered liquid glass with the major components of flux. The formation of complex compounds such as $AlCa_2Mg_5NaSi_7O_{22}F_2$ was supposed. At the temperature above ~1200 °C, the liquid phase is formed due to melting of the liquid glass sinter with the major components and destruction of the complex unstable compounds. The anorthite ($CaAl_2Si_2O_8$) and MgF_2 are formed at the destruction of the complex compounds in the liquid. MgF_2 is the main crystalline phase in the liquid at 1350 °C. The flux melts completely at 1450 °C, but the melt is not homogeneous, since the structure of the upper and inner parts of cooled melt differs markedly. The basicity of the molten surfacing ceramic flux was calculated from data of X-ray study using the technique developed by us. The basicity of the flux melt (found from the X-ray scattering from the surface) is found to be 0.47, and probably somewhat less then that of the inner part of the flux melt, *i.e*. the flux is acidic.

References

[1] Kh. N. Sagirov, D. Kh. Sagirov, S. D. Khachkinaev, S. K. Slitinskaya, N. G. Dyurgerov, D. P. Perfil'ev, Weld. Int., 18 (2004) 121.

[2] P. V. Gladkii, A. P. Zhudra, K. A. Yushchenko,

Surfacing in the U. S. S. R. Welding and Surfacing Reviews, Harwood Academic Publishers, London, UK, 1989.

[3] J. F. Lancaster, Metallurgy of Welding (Welding & Metallurgy), 6th Ed., Abington Publishing, Cambridge, UK, 1999.

[4] A. C. Davies, The Science and Practice of Welding, Vol. 1, Welding Science and Technology, 10th Ed., Cambridge University Press, Cambridge, UK, 1993.

[5] V. Podgaetskii, I. Lyuborets, Svarochnie flyusy (Welding fluxes), Naukova Dumka, Kiev, 1978.

[6] V. Podgaetskii, V. Kuzmenko, Svarochnye Shlaki: Spravochnoe Posobie (Welding Slags. Handbook), Naukova Dumka, Kiev, 1988.

[7] N. N. Potapov, Osnovi vibora flusov pri svarke staley (The base of selecting fluxes in welding of steels), Mashinostroenie, Moscow, 1985.

[8] C. Wagner, Metall. Trans. B., 6 (1975) 405.

[9] C. L. Garey, R. J. Serje, K. Gregory, H. Qinglin, Optical basicity a flexible basis for flux control in steelmaking, in: Proc. of 3rd. Int. Conf. on Molten slags and fluxes, Institute of Metals, Ironmaking and Steelmaking Committee, Société française de métallurgie, London, UK, 1989, p. 157–162.

[10] B. K. Shahraki, B. Mehrabi, K. Gholizadeh, M. Mohammadinasab, J. Min. Metall. Sect. B-Metall., 47 (1) B (2011) 89.

[11] F. Kongoli, I. McBow, R. Budd, S. Llubani, A. Yazawa, J. Min. Metall. Sect. B-Metall., 46(2) B (2010) 123.

[12] W. Kraus, G. Nolze, J. Appl. Cryst., 29 (1996) 301.

[13] http://www.ccp14.ac.uk/ccp/web-mirrors/powdcell/a_v/v_1/powder/e_cell.html

[14] http://www.crystalimpact.com/match/

[15] V. E. Sokol'skii, V. P. Kazimirov, V. G. Kuzmenko, J. Mol. Liq., 93 (2001) 235.

[16] Powder Diffraction File, International Centre for Diffraction Data, ICDD - JCPDS, 1998.

[17] ICSD Database FIZ Karlsruhe, Germany, 2008.

[18] T. Gasparik, Phase Diagrams for Geoscientists, Springer, Berlin, Heidelberg, 2003.

[19] T. Gasparik, J. Geol., 108 (2000) 103.

[20] Slag Atlas, Verlag Stahleisen, Düsseldorf, 1995.

[21] A. S. Berezhnoi, Mnogokomponentnye sistemy okslov (Multicomponent oxide systems), Naukova Dumka, Kiev, 1970.

[22] A. A. Pashchenko, A. A. Myasnikov, E. A. Myasnikova (Eds.), Fizicheskaya Khimiya Silikatov (Physical chemistry of silicates), Vysshaya Shkola, Moscow, 1986.

[23] M. Kumar, S. R. Sankaranarayanan, J. Min. Metall. Sect. B-Metall., 44 B (2008) 133.

[24] D. Ghosh, V. A. Krishnamurthy, S. R. Sankaranarayanan, J. Min. Metall. Sect. B-Metall., 46 (1) B (2010) 41.

[25] A. P. Shpak, V. E. Sokolskii, V. P. Kazimirov, S. Yu. Smyk, Yu. A. Kunitskii, Strukturnye osobennocti rasplavov oksidnykh sistem (Structural features of melts of oxide systems), Akademperiodika, Kiev, 2003.

[26] V. E. Sokolskii, Adv. Electrometallurgy., 51 (1998) 66.

[27] V. E. Sokolskii, V. P. Kazimirov, V. G. Kuzmenko, V. I. Galinich, Izv. Vys. Ucheb. Zav., Chern. Metall., 5 (1999) 3.

[28] V. E. Sokol'skii, V. P. Kazimirov, V. G. Kuzmenko, Adv. Electrometallurgy, 53 (2000) 66.

[29] V. E. Sokol'skii, V. P. Kazimirov, V. A. Shovskii, V. G. Kuzmenko, Russ. J. Appl. Chem., 68 (1995) 1551.